Excited state dynamics of guanosine in aqueous solution revealed by time-resolved photoelectron spectroscopy: experiment and theory

Franziska Buchner,[1] Berit Heggen,[2] Hans-Hermann Ritze,[1] and Walter Thiel[2, 1]

[1]*Max-Born-Institut für nichtlineare Optik und Kurzzeitspektroskopie,*
Max-Born-Straße 2A, 12489 Berlin, Germany.

[2]*Max-Planck-Institut für Kohlenforschung 45470 Mülheim/Ruhr, Germany.*

(Dated: November 11, 2015)

GLOBAL FITTING

For fitting our data we have considered two contributions assigned to excited-state populations, A and B, at two different regions on the S_1 surface. The rate equations describing the excited-state dynamics on the S_1 potential energy surface are given by:

$$\frac{dN_0(t)}{dt} = 0 \tag{S1}$$

$$\frac{dN_A(t)}{dt} = W_{\text{pu}}(t) \cdot N_0 - k_A \cdot N_A(t) \tag{S2}$$

$$\frac{dN_B(t)}{dt} = -k_B \cdot N_B(t) + k_A \cdot N_A(t) \tag{S3}$$

$$n_A(t) = W_{\text{pr}}(t - \Delta t) \cdot N_A(t) \tag{S4}$$

$$n_B(t) = \gamma W_{\text{pr}}(t - \Delta t) \cdot N_B(t) \tag{S5}$$

$N_{A(B)}$ is the number of molecules in the excited state of species A(B). We assume that the excitation is unsaturated, i. e. the number of ground state molecules is not altered significantly by the excitation (N_0 is constant). $W_{\text{pu(pr)}}(t)$ describes the temporal shape of the pump (probe) pulse. We assume that both pulse shapes are Gaussians and their cross-correlation width is ω. The initially populated species A decays with a rate k_A and populates species B, which grows at rate k_A and decays at rate k_B. The probe pulse populates the ionic ground state from species A or B, respectively. This may also proceed via a doubly excited autoionizing state. The ionic population is given by n_A and n_B. The factor γ considers that the two transient species may have different photoionization cross-sections. The solution of this system of differential equations is:

$$S(t) \propto n_A + n_B \tag{S6}$$

$$n_A(t) = \frac{A_0}{2} \cdot \exp\left(\frac{k_A^2 \omega^2}{8} - k_A \Delta t\right) \cdot \text{Erfc}\left(\frac{k_A \omega^2 - 4\Delta t}{2\omega\sqrt{2}}\right) \tag{S7}$$

$$n_B(t) = \frac{\gamma}{2} \cdot \frac{A_0 \cdot k_A}{k_A - k_B}\left(\exp\left(\frac{k_B^2 \omega^2}{8} - k_B \Delta t\right) \cdot \text{Erfc}\left(\frac{k_B \omega^2 - 4\Delta t}{2\omega\sqrt{2}}\right)\right. \tag{S8}$$

$$\left. - \exp\left(\frac{k_A^2 \omega^2}{8} - k_A \Delta t\right) \cdot \text{Erfc}\left(\frac{k_A \omega^2 - 4\Delta t)}{2\omega\sqrt{2}}\right)\right). \tag{S9}$$

We have performed a global fit, i. e. a single set of parameters were fitted to the temporal dependence of the photoelectron signal at a given kinetic energy bin. The amplitude A_0 is thus replaced by a kinetic energy dependent amplitude - the decay associated spectrum

(DAS). For the integrals of the DAS the following relations hold:

$$\int \mathrm{DAS}_A \, \mathrm{d}E_\mathrm{kin} = A_0 \tag{S10}$$

$$\int \mathrm{DAS}_B \, \mathrm{d}E_\mathrm{kin} = \gamma \cdot \frac{A_0 \cdot k_A}{k_A - k_B} \tag{S11}$$

COMPARISON OF DECAY-ASSOCIATED SPECTRA FOR POSITIVE AND NEGATIVE DELAY TIMES

Fig. S1 shows the normalized decay-associated spectra for different wavelength combinations and different pulse sequences. All pairs of spectra are remarkably similar and
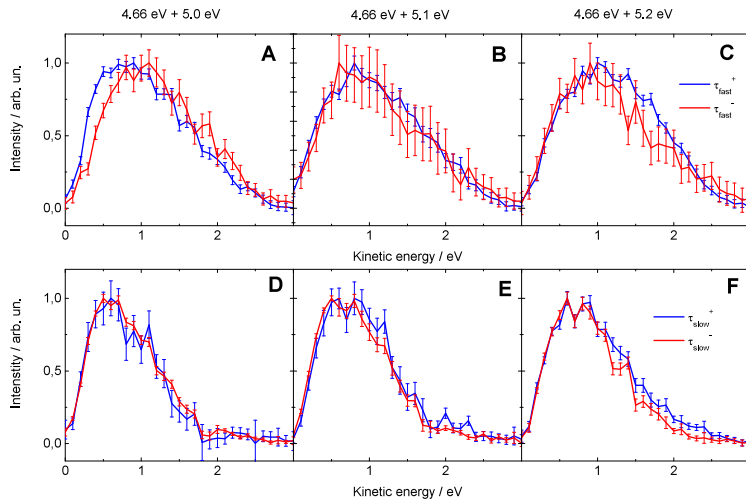

FIG. S1: Comparison of DAS for 4.66 eV and 5.0-5.2 eV pulses with different pulse sequence. Blue: 4.66 eV comes first (positive delays). Red: 5.0-5.2 eV comes first (negative delays). A-C) fast decay. D-F) slow decay.

definitely do not show a shift by the difference of probe photon energy as expected for a vertical transition. While the spectra associated with the slower decay (D-F) are almost identical, we find small differences between the spectra associated with the fast decay. However, these differences are not systematic. We suggest that these differences result from experimental inaccuracy in determining the temporal overlap and cross-correlation function between pump and probe pulses. These values are strongly correlated with the fit parameters associated with the fast decay and much less with those associated with the slow decay. Furthermore, the two components associated with the fast decay are strongly overlapping

at temporal overlap and decomposition is difficult. Nevertheless, a small contribution from direct ionization around temporal overlap cannot be excluded.

COMPUTATION OF IONIZATION POTENTIALS

In the present work, we have evaluated the first ionization potential of 9H-Gua in water for several thousand geometries (130 trajectories, up to 90 points per trajectory) in order to compare with the experimental data (see Figure 3 of the main paper). Our guideline in selecting a computational method for this purpose was to be consistent with the approach used to generate the trajectories (OM2/MRCI) and to apply the simplest treatment that is expected to be realistic. Therefore, our first choice was to apply Koopmans' theorem. At this level, the ionization potential is evaluated by molecular orbital (MO) theory assuming that the MOs do not change during ionization. For closed-shell systems, the ionization potential (IP) is then equal to the negative MO energy: $IP_i = -\epsilon_i$. For restricted open-shell treatments, the derivation yields additional two-electron terms that must be included for proper application of Koopmans' theorem. In our case (open-shell singlet with two unpaired electrons in MOs i and j, $\epsilon_i > \epsilon_j$, half-electron treatment), the appropriate equation is: $IP_i = -\epsilon_i - J_{ii}/4 - J_{jj}/4 + 3K_{ij}/2$, with J and K denoting the Coulomb and exchange integrals in the MO basis. This is the equation applied in our calculations.

An obvious question is whether this approach is adequate for the purposes of the present work (besides being simple and efficient for the very large number of required IP evaluations). This can be checked by higher-level calculations and by comparison with experiment.

Going beyond Koopmans' theorem at the semiempirical OM2 level can be done in two steps. First, one can carry out separate OM2 SCF calculations for the open-shell singlet excited state (S_1) and for the doublet ground state of the cation generated by ionization (D_0) to account for orbital relaxation in the cation, which will cause the resulting OM2-ΔSCF value of the ionization potential to be lower than that given by Koopmans' theorem. In a second step, one can perform corresponding OM2/MRCI calculations of the $D_0 - S_1$ energy difference (using the same active space and the same options as in the trajectory calculations) to include also differences in correlation energy, which will generally raise the computed ionization potential (since ionization removes one electron from the system). The corrections from these two refinements will thus tend to cancel each other – this is the

reason why ionization potentials determined from Koopmans' theorem (KT) are often more realistic than expected.

For a more quantitative assessment, we have computed the ionization potentials of isolated 9H-Gua for two typical geometries taken from a representative trajectory at time $t = 0$ and $t = 100$ fs using the three approaches outlined above (OM2-KT, OM2-ΔSCF, and OM2/MRCI). Those results are summarized in Table S1. For comparison, we have also calculated the $D_0 - S_1$ energy difference of isolated 9H-Gua at these two geometries by density functional theory (DFT) at the B3LYP/TZVP level (TDDFT for S_1, UDFT for D_0).

	$IP(t = 0)$ / eV	$IP(t = 100)$ fs / eV	Difference / eV
OM2-KT	3.57	5.06	1.49
OM2-ΔSCF	3.48	4.87	1.39
OM2/MRCI	3.93	5.24	1.31
B3LYP/TZVP	3.39	4.42	1.03

TABLE S1: Calculated ionization potentials of the S_1 state of 9H-Gua.

Evidently, all approaches yield ionization potentials of roughly similar magnitude, and they all predict a significant increase within the first 100 fs of the excited-state dynamics.

Experimentally, this increase is clearly observed and is of similar magnitude (see Figure 3 of the main paper). All approaches considered thus agree with experiment in this crucial qualitative aspect. To achieve a more quantitative fit, the OM2-KT values were calibrated against experiment (uniform shift of -1.0 eV, see the main paper) which gave a very satisfactory match with experiment (see Figure 3b of the main paper). To achieve a better quantitative agreement without calibration, it would be necessary to apply significantly more accurate computational methods (DFT at the B3LYP/TZVP would not be sufficient for this purpose, see the results in Table S1). This is beyond the scope of the present computational work, which focuses on a qualitative understanding of the experimental observations.

In summary, these considerations and comparisons justify the application of Koopmans' theorem at the OM2 level to compute the time evolution of the ionization potential of 9H-Gua in water during the excited-state dynamics.

AB-INITIO RESULTS

The ab initio calculations and their interpretation were performed at MBI Berlin. For an evaluation of energies and transition dipole moments the MOLPRO program package was used [S1]. We have employed the aug-cc-pVTZ basis set. In CASSCF calculations three active orbitals were selected: HOMO, LUMO and LUMO+1. Under these circumstances the third excited state is the lowest doubly excited state. The CASSCF calculations were followed by the MRCI procedure - more precisely MRCISD(+Q) (with Davidson correction). The geometries investigated are documented in tables S3-S8 in the final section of this Supporting information.

Table S2 summarizes our ab-initio results on the accessibility of a doubly-excited state. The potential energies are also displayed in Fig. S2. It must be noted that the behaviour of the specified electronic state can only be interpreted qualitatively. In the first instance, quantitative discrepancies may be explained by the absence of the water environment. Eventually, the S_1 and 2xEx potential energies given in Fig. S2 should be lowered by $0.5 \ldots 1\,\mathrm{eV}$ to produce realistic results. Fig. S3 shows the CASSCF HOMO (π) and LUMO (π^*) orbitals.

	S_0	S_1	2xEx	D_0	Δ	$E_{\mathrm{kin}}^{\mathrm{theo}}$	$|\mu|_{S_0 \leftrightarrow S_1}$	$|\mu|_{S_1 \leftrightarrow 2\mathrm{Ex}}$
eq. geom.	0	4.80	10.05	7.32	5.25	2.73	0.15	3.3
geom. 1	2.25	6.18	10.39	8.89	4.21	1.50		2.8
geom. 2	3.84	7.02	11.60	11.10	4.58	0.50	not relevant	1.4
geom. 3	3.13	6.42	11.04	9.81	4.62	1.23		0.7
geom. 4	2.42	6.14	10.86	9.73	4.72	1.13		0.7
geom. 5	4.00	5.99	10.69	10.61	4.70	0.08		0.6

TABLE S2: Calculated MRCI energies of S_0, S_1, the doubly excited state (2Ex) and the lowest ionic state in eV. Δ is the potential energy difference between S_1 and 2xEx and $E_{\mathrm{kin}}^{\mathrm{theo}}$ is the potential energy difference between the lowest doubly excited and the ionic D_0 state. Calculated transition dipole moments are given in Debye.
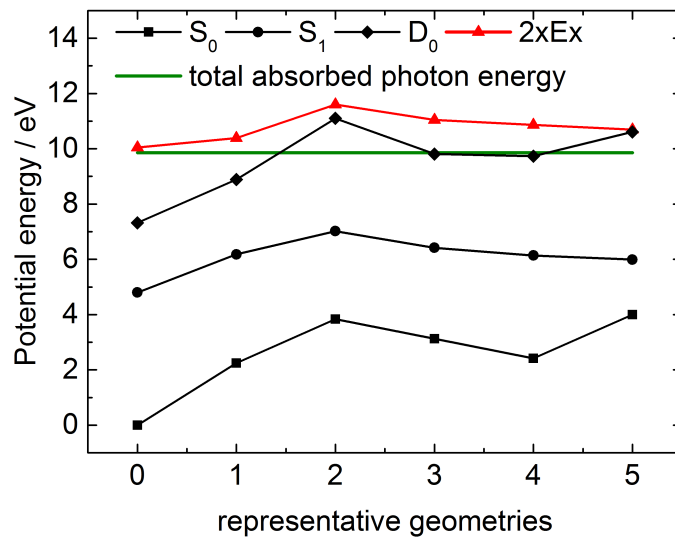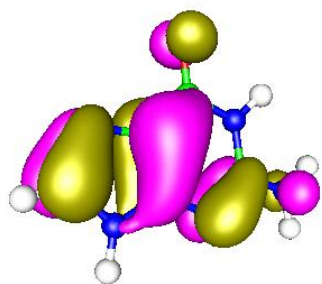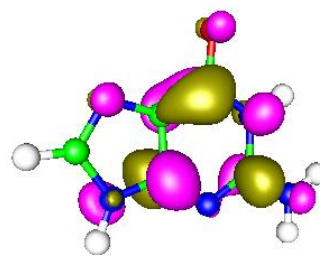
FIG. S2: Potential energies of the S_0, S_1, the lowest doubly excited 2xEx and the ionic D_0 state for different representative geometries along a representative trajectory (from table S2). The green line represents the total absorbed photon energy.

a)   b)

FIG. S3: CASSCF orbitals of guanine ($t = 0$) for HOMO (π) (a) and LUMO (π^*) (b).

ANALYTICAL CONSIDERATIONS

In this section we will show that the kinetic energy distribution observed for direct ionization and autoionization depend differently on the applied photon energies. Let's consider the potential energy landscape sketched in Fig. S4. From energy conservation and Fig. S4
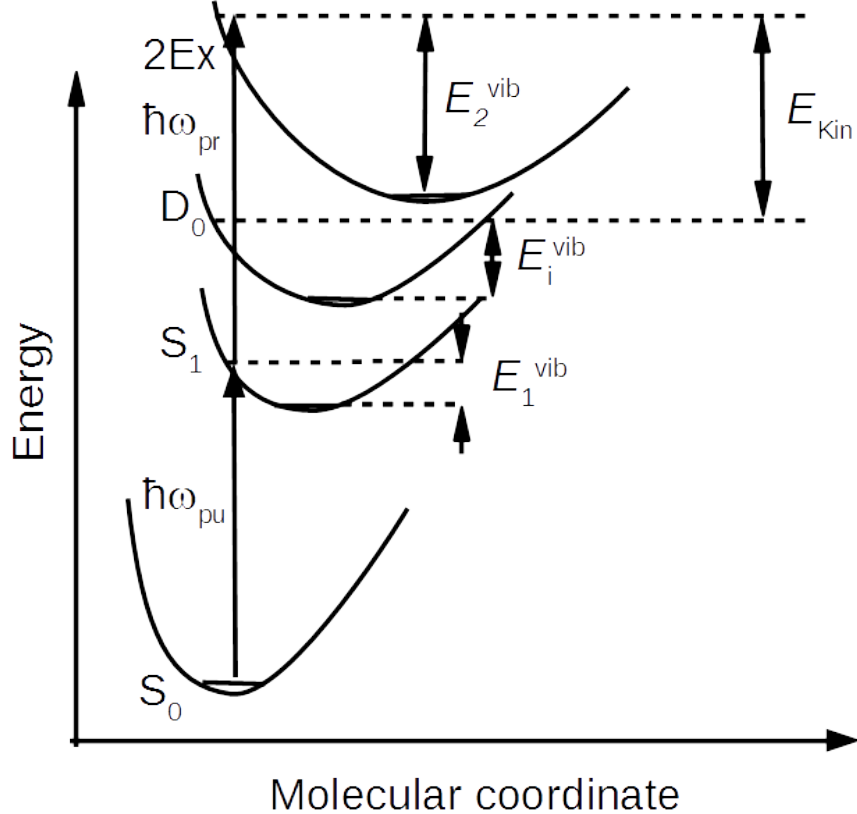

FIG. S4: Involved potentials to explain autionization and direct ionization. $\hbar\omega_{\mathrm{pu}}$ and $\hbar\omega_{\mathrm{pr}}$ are the pump and probe photon energies, E_{S_1}, E_{2Ex} and E_{D_0} the energies of the minima (+ zero-point-energy) of the S_1, 2Ex and D_0 electronic states relative to S0. E_1^{vib}, E_2^{vib}, and $E_{\mathrm{i}}^{\mathrm{vib}}$ are the vibrational energies stored in the S_1, 2Ex and D_0 electronic states. E_{kin} is the kinetic energy of the photoelectrons.

we derive the following relations:

$$\begin{aligned} \hbar\omega_{\mathrm{pu}} &= E_{\mathrm{S}_1} + E_1^{\mathrm{vib}} \\ \hbar\omega_{\mathrm{pu}} + \hbar\omega_{\mathrm{pr}} &= E_{\mathrm{D}_0} + E_{\mathrm{i}}^{\mathrm{vib}} + E_{\mathrm{kin}} \end{aligned} \tag{S12}$$

In general, due to the finite Franck-Condon window, after ionization several vibrational levels are excited. From eq. (S12) the following relation between the mean kinetic energy of

photoelectrons $\overline{E_{\mathrm{kin}}}$ and the mean vibrational energy in the cation $\overline{E_i^{\mathrm{vib}}}$ follows:

$$\overline{E_{\mathrm{kin}}} = \hbar\omega_{\mathrm{pr}} + E_{S_1} - E_{D_0} + (E_1^{\mathrm{vib}} - \overline{E_i^{\mathrm{vib}}}). \tag{S13}$$

In case of direct ionization, $(E_1^{\mathrm{vib}} - \overline{E_i^{\mathrm{vib}}})$ can be obtained from the Franck-Condon overlap, if the S_1 and D_0 potential surfaces are known. For a vertical transition $(E_1^{\mathrm{vib}} - \overline{E_i^{\mathrm{vib}}})$ is almost independent of $\hbar\omega_{\mathrm{pr}}$, and the mean kinetic energy increases with increasing probe photon energy.

The situation is different in case of autoionization. From Fig. S4, we derive the following relation:

$$\hbar\omega_{\mathrm{pu}} + \hbar\omega_{\mathrm{pr}} = E_{2\mathrm{Ex}} + E_2^{\mathrm{vib}} = E_{D_0} + E_i^{\mathrm{vib}} + E_{\mathrm{kin}}. \tag{S14}$$

The mean kinetic energy in this case is therefore given by:

$$\overline{E_{\mathrm{kin}}} = E_{2\mathrm{Ex}} - E_{D_0} + (E_2^{\mathrm{vib}} - \overline{E_i^{\mathrm{vib}}}). \tag{S15}$$

Comparing eq. (S13) and (S15) we obtain that $\overline{E_{\mathrm{kin}}}$ is the same for direct ionization and autoionization if the 2Ex potential surface is parallel to S_1 and furthermore the relation

$$\hbar\omega_{\mathrm{pr}} = E_{2\mathrm{Ex}} - E_{S_1} \tag{S16}$$

is fulfilled which is compatible with our ab-initio calculations.

For a more detailed discussion we will further simplify our model and consider only one vibrational degree of freedom. All electronic states are approximated by harmonic oscillators of the same frequency ω_0. This allows an easy calculation of the overlap matrix elements between a state of vibrational quantum number v with a state of quantum number w in a potential shifted by the distance Δq. Introducing the dimensionless quantity

$$\Delta x = \Delta q \sqrt{\frac{\mu\omega_0}{\hbar}}, \tag{S17}$$

where μ is the reduced mass, we define (cf. Fig. S5)

$$f_{v-w}(\Delta x) = \left\langle \Psi_v^{(1)} | \Psi_w^{(2)} \right\rangle, \tag{S18}$$

which yields [S2]:

$$f_{v-w}(\Delta x) = \sqrt{\frac{v!}{w!}} \left(\frac{\Delta x}{\sqrt{2}}\right)^{w-v} e^{-\frac{(\Delta x)^2}{4}} L_v^{w-v}\left[\frac{(\Delta x)^2}{2}\right], \tag{S19}$$
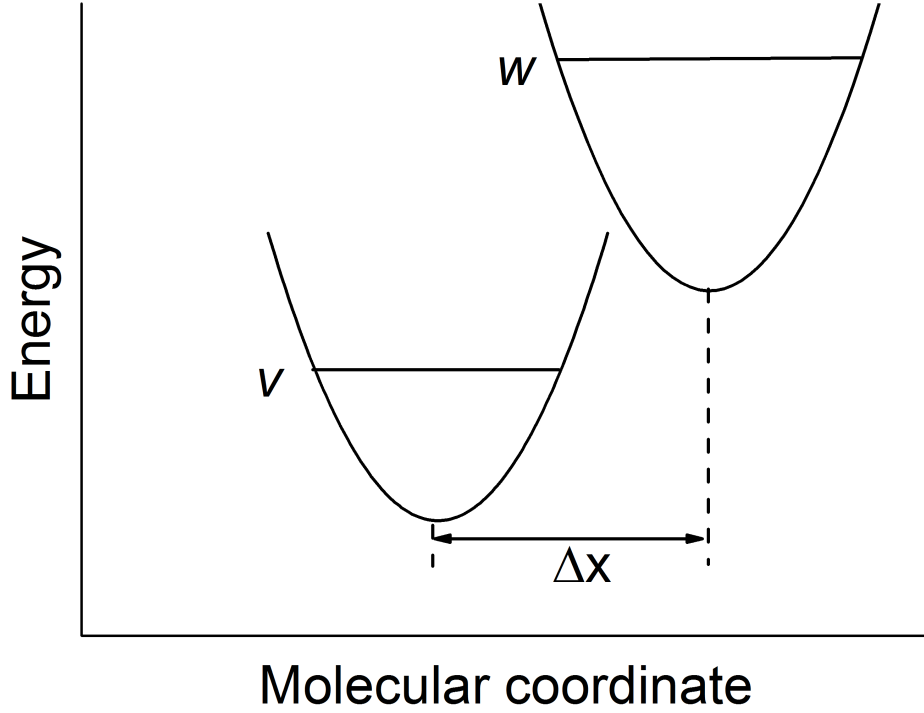
FIG. S5: Most simple approximation of the potentials involved: One-dimensional harmonic potentials of the same shape.

where $L_n^\alpha(z) = \sum_{m=0}^n (-1)^m \binom{n+\alpha}{n-m} \frac{z^m}{m!}$ is the associated Lagurerre polynomial. Assuming an infinite Franck-Condon window for the transition from the initial state $|v\rangle$ to the final state $|w\rangle$, the average quantum number of the final state can be expressed as

$$\overline{w} = \sum_{w=0}^\infty w \left| f_{v-w}(\Delta x) \right|^2 = v + \frac{(\Delta x)^2}{2}. \tag{S20}$$

However, the Franck-Condon window is limited, due to $E_{\text{kin}} \geq 0$. If we consider an autoionization process with $E_{\text{2Ex}} - E_{\text{D}_0} = n\hbar\omega_0$, we can write

$$\overline{w} = \frac{\sum_{w=0}^{n+v} w \left| f_{v-w}(\Delta x) \right|^2}{\sum_{w=0}^{n+v} \left| f_{v-w}(\Delta x) \right|^2}. \tag{S21}$$

For the example $n = 10$, the dependence of $\overline{w} - v$ on the initial quantum number v is shown in Fig. S6 for different values (Δx). Since $E_2^{\text{vib}} = v\hbar\omega_0$, and $\overline{E_i^{\text{vib}}} = \overline{w}\hbar\omega_0$ we find from Fig.

S6, that the limitation of the Franck-Condon window causes a dependence of $\overline{E_{kin}}$ on the total absorbed photon energy. This effect is more pronounced for larger values (Δx).
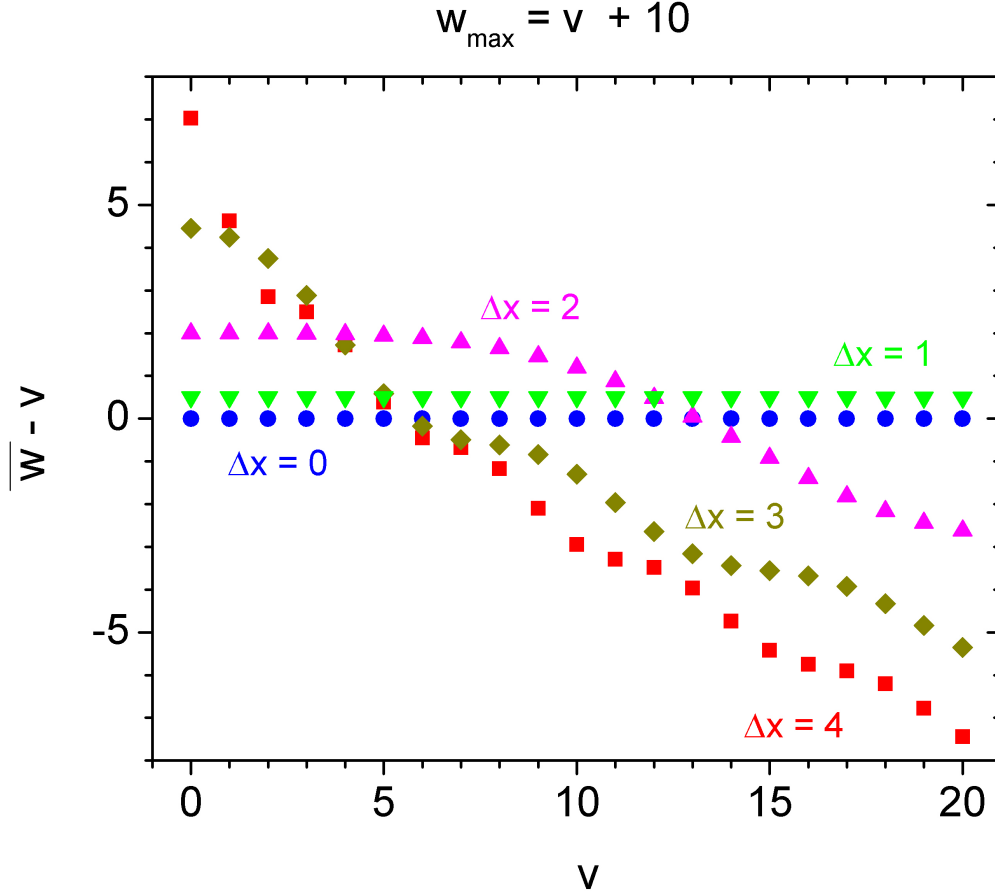
FIG. S6: The difference between mean vibrational energy in the ionic state and the vibrational energy in the autoionizing state for different number of vibrational quanta in the initial state and for different displacements of the two potentials.

So far, we restricted our considerations to only one vibrational degree of freedom. We will now turn to the more general case with more than one vibrational degree of freedom. Here, we restrict ourselves to equal harmonic vibrational frequencies ω_0.

If the potential is shifted by the same amount (Δx) for all N vibrational degrees of freedom, the problem can be reduced again to the one-dimensional case: Due to the N-dimensional degeneracy, new vibrational coordinates can be introduced in such a way, that for $N-1$ vibrational degrees $\Delta x_{new} = 0$, and for the last vibrational degree we obtain

$\Delta x_{\text{new}} = \Delta x \sqrt{N}$. Therefore, new features can only be expected if the shift of a potential relative to the reference ground state potential depends on the vibrational degree of freedom. As an example, we choose $N = 3$. The S_1 potential is shifted relative to S_0 by Δx_1, Δx_2 and Δx_3. The 2Ex shift from S_0 is given by Δy_1, Δy_2 and Δy_3, for D_0 we write correspondingly Δz_1, Δz_2 and Δz_3. In an autoionization process via 2Ex, the probability to find t quanta in D_0, if r vibrational quanta are located in S_1 and s in 2Ex, is proportional to

$$p_{\text{auto}}(r, s, t) = \left[\sum_{r_1, r_2, s_1, s_2, t_1, t_2} f_{0 \leftrightarrow r_1}(\Delta x_1) f_{0 \leftrightarrow r_2}(\Delta x_2) f_{0 \leftrightarrow r - r_1 - r_2}(\Delta x_3) \times \right. \tag{S22}$$
$$\times\, f_{r_1 \leftrightarrow s_1}(\Delta y_1 - \Delta x_1) f_{r_2 \leftrightarrow s_2}(\Delta y_2 - \Delta x_2) f_{r - r_1 - r_2 \leftrightarrow s - s_1 - s_2}(\Delta y_3 - \Delta x_3) \times$$
$$\left. \times\, f_{s_1 \leftrightarrow t_1}(\Delta z_1 - \Delta y_1) f_{s_2 \leftrightarrow t_2}(\Delta z_2 - \Delta y_2) f_{s - s_1 - s_2 \leftrightarrow t - t_1 - t_2}(\Delta z_3 - \Delta y_3) \right]^2$$

The mean kinetic energy of photoelectrons can be determined if the mean number of vibrational quanta $\overline{t_{\text{auto}}}$ in the ionic state is known, where

$$\overline{t_{\text{auto}}}(r, s) = \frac{\sum_{t=0}^{t=n+s} t \cdot w_{\text{auto}}(r, s, t)}{\sum_{t=0}^{t=n+s} w_{\text{auto}}(r, s, t)} \tag{S23}$$

In contrast to eq. (S23), the corresponding probability for direct ionization can be expressed by

$$p_{\text{ion}}(r, t) = \left[\sum_{r_1, r_2, t_1, t_2} f_{0 \leftrightarrow r_1}(\Delta x_1) f_{0 \leftrightarrow r_2}(\Delta x_2) f_{0 \leftrightarrow r - r_1 - r_2}(\Delta x_3) \times \right. \tag{S24}$$
$$\left. \times\, f_{r_1 \leftrightarrow t_1}(\Delta z_1 - \Delta x_1) f_{r_2 \leftrightarrow t_2}(\Delta z_2 - \Delta x_2) f_{r - r_1 - r_2 \leftrightarrow t - t_1 - t_2}(\Delta z_3 - \Delta x_3) \right]^2$$

with the mean quantum number

$$\overline{t_{\text{ion}}}(r) = \frac{\sum_{t=0}^{t=n+r} t \cdot w_{\text{ion}}(r, t)}{\sum_{t=0}^{t=n+r} w_{\text{ion}}(r, t)} \tag{S25}$$

In eq. (S23) we set $E_{2\text{Ex}} - E_{D_0} = n\hbar\omega_0$, whereas in eq. (S25) the requirement $E_{\text{kin}} \geq 0$ is ensured by the condition $E_{S_1} - E_{D_0} + \hbar\omega_{\text{pr}} = n\hbar\omega_0$. As a simple example, we set $n = 10$ and $\Delta x_1 = 1.0$, $\Delta x_2 = 2.0$, $\Delta x_3 = 3.0$, $\Delta y_2 = 3.0$, $\Delta y_3 = 4.0$, $\Delta z_1 = 3.5$, $\Delta z_2 = 2.5$, $\Delta z_3 = 1.5$. Using these specified parameters we will compare the vibrational energy in the D_0 state for direct ionization and autoionization in dependence on the vibrational energy in the S_1 (and 2Ex) state. The results are outlined in Fig. S7. For direct ionization, the vibrational energy in the ion increases approximately by the same number of quanta as the vibrational energy
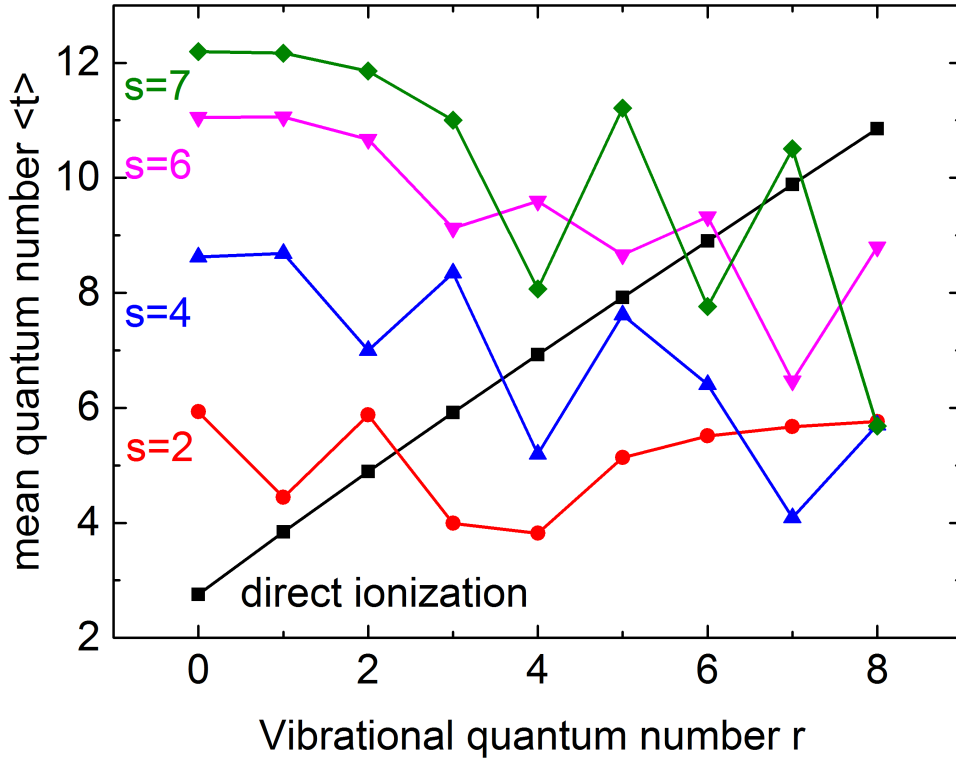
FIG. S7: Mean number of vibrational quanta in the ion as function of the vibrational quantum number in the S_1 state for different vibrational excitation of the 2Ex state for direct ionization and autoionization

in the S_1 state. The situation is qualitatively different for autoionization from the 2Ex state. Here, we do not observe any clear tendency for several quanta vibrational energy s in the 2Ex state. For a given s value there are several r values yielding nearly the same vibrational excitation in the ion (as in the one-dimensional case), however, other r values unreeve.

GEOMETRIES USED IN THE AB INITIO CALCULATIONS

Eq. geometry

Number	Atom	Charge	X	Y	Z
1	N	7.00	−0.216 307 539	−6.158 541 741	−3.052 143 937
2	C	6.00	0.457 345 603	−3.728 121 443	−2.520 644 856
3	N	7.00	−1.140 799 584	2.399 918 191	−0.463 170 930
4	H	1.00	−0.347 512 793	4.090 896 345	−0.087 543 963
5	H	1.00	−2.959 393 552	2.200 844 954	0.013 691 935
6	N	7.00	−1.040 970 323	−1.836 321 318	−1.646 925 047
7	C	6.00	0.188 704 007	0.383 809 235	−1.306 507 514
8	N	7.00	2.731 785 677	0.728 922 946	−1.820 621 417
9	H	1.00	3.532 639 215	2.477 095 381	−1.526 139 989
10	C	6.00	4.355 351 838	−1.190 794 217	−2.641 636 348
11	O	8.00	6.660 194 355	−0.723 494 934	−2.952 686 082
12	C	6.00	3.123 354 997	−3.570 284 033	−3.068 243 837
13	N	7.00	3.958 980 781	−5.883 541 046	−3.897 766 013
14	C	6.00	1.940 140 264	−7.402 740 279	−3.875 332 280
15	H	1.00	1.909 652 292	−9.374 726 737	−4.398 750 835
16	H	1.00	−1.954 982 230	−7.006 885 060	−2.791 793 061

TABLE S3: Coordinates for equilibrium geometry in bohr.

geom. 1

NR	ATOM	CHARGE	X	Y	Z
1	N	7.00	−0.410 085 688	−6.152 419 161	−2.257 687 935
2	C	6.00	−0.258 648 705	−3.513 832 358	−2.050 239 469
3	N	7.00	−3.562 715 793	1.863 084 772	−0.777 879 306
4	H	1.00	−3.562 182 891	3.717 289 722	−1.277 396 283
5	H	1.00	−5.181 908 732	1.188 278 689	−0.069 160 197
6	N	7.00	−2.216 355 845	−2.206 667 219	−1.376 306 439
7	C	6.00	−1.683 944 404	0.375 190 006	−1.691 114 025
8	N	7.00	0.288 606 534	1.456 534 762	−2.918 693 348
9	H	1.00	0.348 219 834	3.395 718 805	−3.319 940 788
10	C	6.00	2.852 915 761	0.038 034 518	−2.867 060 361
11	O	8.00	4.670 348 530	0.996 063 306	−3.866 396 672
12	C	6.00	2.386 691 979	−2.885 557 001	−2.824 161 688
13	N	7.00	3.344 654 626	−4.910 413 668	−4.022 533 404
14	C	6.00	1.783 514 074	−6.863 919 946	−3.505 181 192
15	H	1.00	1.980 929 984	−8.821 714 013	−4.159 933 502
16	H	1.00	−1.962 121 540	−7.310 815 610	−1.734 386 864

TABLE S4: Coordinates for geometry 1 in bohr.

geom. 2

NR	ATOM	CHARGE	X	Y	Z
1	N	7.00	−0.514 339 989	−6.063 843 917	−2.338 796 870
2	C	6.00	−0.120 623 109	−3.475 374 541	−2.132 931 995
3	N	7.00	−3.598 085 797	2.041 692 238	−1.430 877 950
4	H	1.00	−3.768 813 105	3.878 241 476	−1.730 376 865
5	H	1.00	−4.732 758 625	1.673 554 690	0.035 725 273
6	N	7.00	−1.931 322 783	−1.790 156 462	−1.126 102 920
7	C	6.00	−1.458 288 428	0.607 490 259	−1.721 464 917
8	N	7.00	0.406 281 670	1.402 161 672	−3.220 888 903
9	H	1.00	−0.011 018 993	2.897 055 984	−4.463 805 243
10	C	6.00	2.814 318 105	0.259 451 839	−3.001 257 373
11	O	8.00	4.369 838 611	1.116 790 349	−4.602 310 830
12	C	6.00	2.635 410 173	−2.941 695 095	−2.759 584 077
13	N	7.00	3.463 987 052	−4.897 153 460	−4.007 011 194
14	C	6.00	1.623 206 717	−6.743 752 262	−3.783 751 390
15	H	1.00	1.871 762 395	−8.744 380 751	−4.429 126 879
16	H	1.00	−2.092 093 123	−7.146 781 713	−1.908 118 836

TABLE S5: Coordinates for geometry 2 in bohr.

geom. 3

NR	ATOM	CHARGE	X	Y	Z
1	N	7.00	−0.272 874 564	−6.031 495 585	−2.298 507 909
2	C	6.00	−0.203 170 126	−3.389 276 729	−2.291 568 834
3	N	7.00	−3.343 229 772	2.384 838 157	−1.512 047 357
4	H	1.00	−3.065 373 891	4.211 010 909	−1.640 631 881
5	H	1.00	−5.082 097 177	1.991 818 586	−0.900 057 659
6	N	7.00	−1.838 648 724	−1.812 606 408	−1.247 160 665
7	C	6.00	−1.307 286 082	0.763 266 054	−1.831 263 674
8	N	7.00	0.787 923 200	1.825 683 313	−3.040 644 935
9	H	1.00	0.519 051 077	3.642 934 668	−3.798 495 033
10	C	6.00	3.099 717 773	0.462 041 819	−3.582 735 552
11	O	8.00	4.539 262 007	0.902 501 075	−5.273 420 609
12	C	6.00	2.324 941 398	−2.722 014 432	−3.227 661 681
13	N	7.00	3.458 563 538	−4.696 479 663	−4.143 419 185
14	C	6.00	1.962 983 255	−6.631 194 504	−3.683 869 915
15	H	1.00	2.376 840 836	−8.718 064 424	−3.711 745 265
16	H	1.00	−1.713 909 792	−7.279 138 131	−1.692 684 388

TABLE S6: Coordinates for geometry 3 in bohr.

geom. 4

NR	ATOM	CHARGE	X	Y	Z
1	N	7.00	−0.187 487 288	−5.677 532 873	−2.575 133 579
2	C	6.00	0.066 361 513	−3.057 752 625	−2.493 123 244
3	N	7.00	−2.948 105 046	2.687 523 151	−1.277 366 048
4	H	1.00	−2.584 559 533	4.559 695 616	−1.004 272 276
5	H	1.00	−4.802 846 677	2.168 844 350	−1.024 960 998
6	N	7.00	−1.904 942 206	−1.558 392 890	−1.924 128 596
7	C	6.00	−1.227 877 900	0.960 132 053	−1.908 921 969
8	N	7.00	1.124 281 224	1.701 713 499	−2.777 377 739
9	H	1.00	1.245 369 205	3.585 585 259	−2.842 990 920
10	C	6.00	3.276 743 538	0.148 358 619	−3.637 711 465
11	O	8.00	4.282 945 224	0.735 275 430	−5.750 054 893
12	C	6.00	2.771 432 660	−2.684 926 667	−3.292 872 350
13	N	7.00	3.612 396 693	−4.950 492 870	−4.209 671 093
14	C	6.00	1.870 428 248	−6.777 631 272	−3.762 425 830
15	H	1.00	2.438 311 738	−8.841 044 022	−3.764 852 239
16	H	1.00	−1.633 025 734	−6.753 185 774	−2.429 231 604

TABLE S7: Coordinates for geometry 4 in bohr.

geom. 5

NR	ATOM	CHARGE	X	Y	Z
1	N	7.00	−0.365 684 683	−5.580 172 293	−3.505 426 856
2	C	6.00	−0.148 638 299	−3.094 619 292	−2.910 569 416
3	N	7.00	−2.520 586 634	2.643 316 787	−1.173 366 860
4	H	1.00	−2.059 310 154	4.536 580 486	−1.032 442 423
5	H	1.00	−4.269 960 916	2.013 554 216	−0.575 200 509
6	N	7.00	−1.561 121 654	−1.454 433 386	−1.621 490 845
7	C	6.00	−0.666 655 695	1.050 387 263	−1.840 022 555
8	N	7.00	1.612 578 897	1.848 103 024	−2.524 649 545
9	H	1.00	1.765 317 901	3.729 773 253	−2.661 737 838
10	C	6.00	3.669 209 420	0.186 085 112	−3.423 518 567
11	O	8.00	4.211 475 782	0.880 122 938	−5.568 969 997
12	C	6.00	2.610 815 388	−2.630 961 758	−3.064 876 893
13	N	7.00	3.793 024 276	−4.824 521 836	−3.562 693 117
14	C	6.00	2.057 677 431	−6.661 346 974	−4.012 497 069
15	H	1.00	2.477 221 199	−8.683 677 078	−4.154 098 027
16	H	1.00	−1.848 926 944	−6.318 295 541	−4.082 275 206

TABLE S8: Coordinates for geometry 5 in bohr.

[S1] H.-J. Werner, P. J. Knowles, G. Knizia, F. R. Manby, and M. Schütz, Wiley Interdisciplinary Reviews: Computational Molecular Science **2**, 242 (2012).

[S2] I. S. Gradshteyn and I. M. Ryzhik, *Tables of Integrals, Series, and Products, 7th edition* (Elsevier Amsterdam, 2007).